J|A|C|S
ARTICLES
Published on Web 02/19/2002

Quantitative Cavities and Reactivity in Stages of Crystal Lattices: Mechanistic and Exploratory Organic Photochemistry[1,2]

Howard E. Zimmerman* and Evgueni E. Nesterov

Contribution from the Chemistry Department of the University of Wisconsin, Madison, Wisconsin, 53706

Received October 29, 2001. Revised Manuscript Received December 21, 2001

Abstract: In continuing our research on solid-state organic photochemistry, we have been investigating the phenomenon of reactivity in stages. In this study we present new examples where the photochemical reactivity changes discontinuously at some point in the conversion. In these instances, the reaction course of the solid differs from that in solution. One example is the reaction of 2-methyl-4,4-diphenylcyclohexenone, where an unusual reaction course was encountered in the solid state; and, of two possible mechanisms, one was established by isotopic labeling. A second case is that of 4,5,5-triphenylcyclohexenone. The solid-state reaction of this enone was found to give a new photochemical transformation, the Type C rearrangement, a process that involves a δ to α aryl migration. In the case of 3-*tert*-butyl-5,5-diphenylcyclohexenone the Type C rearrangement occurred even in solution. The stage behavior was investigated using X-ray analysis and Quantum Mechanics/Molecular Mechanics computations. This permitted us to determine the sources and details of the stage phenomenon. The analysis revealed how a product molecule as a neighbor affects reactivity. The computations were employed to follow the course of a solid-state reaction from reactant through the succeeding stages. Additionally, the Delta-Density Analysis was utilized to ascertain the electronic nature of molecular changes. Besides product composition changing with extent of conversion, the reaction quantum yield was found to change as one stage gave way to a succeeding one.

Introduction

Our research in solid-state photochemistry began 15 years ago with the philosophy of treating crystal-lattice photochemistry quantitatively. One major objective dealt with the pioneering research of Cohen and Schmidt, who noted that the reaction of a molecule can be envisioned as taking place in a cavity composed of surrounding molecules of the lattice.[3] This qualitative, but invaluable, concept has been invoked in the last four decades in a myriad of solid-state photochemical studies. Surprisingly, despite the availability of X-ray structures, the cavity concept remained qualitative. Thus, in our initial crystal-lattice studies we concluded that, with the coordinates of all atoms surrounding a single lattice molecule known, the cavity could be defined quantitatively.[4] Computational extraction of one molecule leaves the cavity, which then is quantitatively defined by the coordinates of the nearest atoms of the surrounding molecules. We defined a subset of the X-ray crystal lattice as a "mini-crystal lattice".

Our initial efforts focused on the "fit" of a reacting species in the cavity of the mini-crystal lattice. "Fit" was gauged by the overlap of the reacting species with the surrounding lattice.[4] These initial, somewhat primitive, efforts were followed by estimation of the energy of the reacting molecule by molecular mechanics.[5,6] But with the realization that molecular mechanics omitted the electron delocalization effect, in subsequent efforts, we constructed the cavity with an inert gas shell obtained by replacing the nearest neighboring atoms by heliums for hydrogens and neons for carbon, oxygen, and nitrogen. With this irregularly shaped cavity shell held rigid, it was possible to treat the imbedded reacting molecule quantum mechanically.[7] Most recently,[8,9] we have made use of the combined QM/MM (ONIOM) programming by Morokuma[10] as imbedded in Gauss-

* Address correspondence to this author. E-mail: zimmerman@chem.wisc.edu.

(1) This is Paper 197 of our photochemical series and Paper 264 of our general series.
(2) (a) For Paper 262 see: Zimmerman, H. E.; Wang, P. *Helv. Chim. Acta* **2001**, *84*, 1342−1346. (b) For a preliminary Communication of a portion of the present results see: Zimmerman, H. E.; Nesterov, E. E. *Org. Lett.* **2000**, *2*, 1169−1171.
(3) (a) Cohen, M. D.; Schmidt, G. M. J. *J. Chem. Soc.* **1964**, 1996−2000. (b) Cohen, M. D. *Angew. Chem., Int. Ed. Engl.* **1975**, *14*, 386−393.
(4) (a) Zimmerman, H. E.; Zuraw, M. J. *J. Am. Chem. Soc.* **1989**, *111*, 2358−2361. (b) Zimmerman, H. E.; Zuraw, M. J. *J. Am. Chem. Soc.* **1989**, *111*, 7974−7989.
(5) (a) Zimmerman, H. E.; Zhu, Z. *J. Am. Chem. Soc.* **1994**, *116*, 9757−9758. (b) Zimmerman, H. E.; Zhu, Z. *J. Am. Chem. Soc.* **1995**, *117*, 5245−5262.
(6) Zimmerman, H. E.; Sebek, P. *J. Am. Chem. Soc.* **1997**, *119*, 3677−3690.
(7) Zimmerman, H. E.; Sebek, P.; Zhu, Z. *J. Am. Chem. Soc.* **1998**, *120*, 8549−8550.
(8) Zimmerman, H. E.; Alabugin, I. V.; Smolenskaya, V. N. *Tetrahedron* **2000**, *56*, 6821−6831.
(9) Zimmerman, H. E.; Alabugin, I. V.; Chen, W.; Zhu, Z. *J. Am. Chem. Soc.* **1999**, *121*, 11930−11931.
(10) (a) Maseras, F.; Morokuma, K. *J. Comput. Chem.* **1995**, *16*, 1170−1179. (b) Matsubara, T.; Sieber S.; Morokuma, K. *Int. J. Quantum Chem.* **1996**, *60*, 1101−1109.

10.1021/ja0124562 CCC: $22.00

Scheme 1. Synthesis of *tert*-Butyl Enone **4**

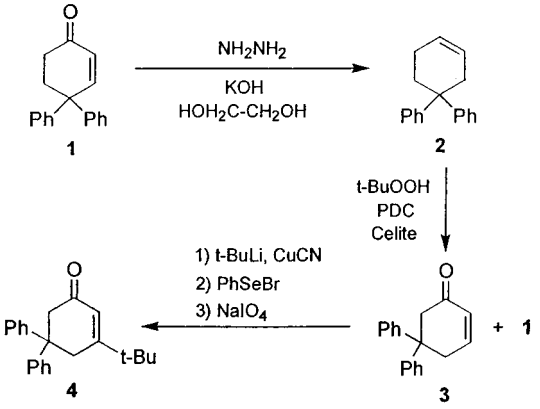

Scheme 2. Synthesis of the C-13 Labeled 2-Methyl Enone **9**

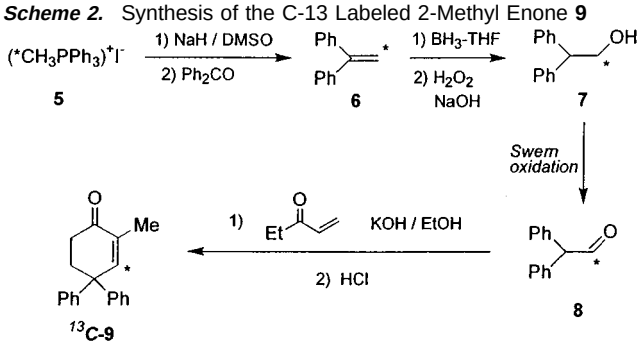

Scheme 3. Synthesis of Photoproduct **14**

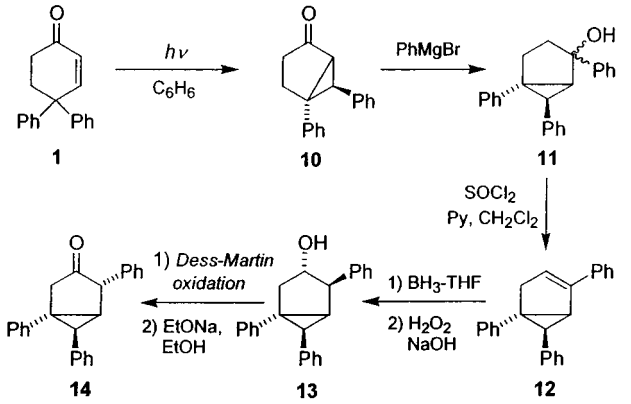

ian 98.[11] This permitted us to treat the reacting molecule with ab initio quantum mechanics while treating the surrounding molecules with molecular mechanics.[8,9] This also enabled quantitative assessment of crystal relaxation effects.

With this methodology available we proceeded to investigate a number of further solid-state reactions and encountered a remarkable phenomenon.[2b] Hitherto, it has been assumed that solid-state reactions sometimes could be brought to high conversions, but that more often at some point the crystal structure is lost and the reaction leads to a heterogeneous, useless aggregate. Our finding was that crystal lattice reactions often proceed in stages, and that in those subsequent stages different and useful products tend to be formed. The present paper deals with that phenomenon and also describes a number of new reactions and their theoretical treatment.

Results

(A) Synthesis. The present study required a number of photochemical reactants as well as the independent synthesis of certain photoproducts. Thus three syntheses are noteworthy and are given in Schemes 1−3. In the case of the synthesis of *tert*-butyl enone **4**, allylic oxidation of cyclohexene **2** did afford the desired enone **3**; however, this was a minor product (ca. 25%); and enone **1** resulted as the major product. Nevertheless, the diphenylcyclohexenone **1** formed was just recycled, and thus the synthesis proved to be practical.

A second synthesis was of ^{13}C-labeled 2-methyl enone **^{13}C-9.** This was required for mechanistic studies (vide infra). A practical synthesis began with ^{13}C-labeled methyl iodide and thence via formation of the phosphonium salt, the Wittig reaction, hydroboration, Swern oxidation, and Robinson annelation led nicely to the required 2-methyl product uniquely labeled at C3. This is outlined in Scheme 2.

A more difficult synthesis was required for preparation of an unusual bicyclic photoproduct **14**. This synthesis is outlined in Scheme 3. The elimination step, involving conversion of **11** to **12**, proved difficult, primarily due to opening of the three-membered ring under most conditions. However, a simple thionyl chloride reaction under the conditions shown afforded practical yields along with an equal amount of 1,3,4-triphenylcyclohexa-1,4-diene (**15**). Another problem was encountered in this synthesis: most oxidative conditions failed for the conversion of the triphenylbicyclohexanol **13** to the corresponding ketone (Swern oxidation, PCC, and most other CrO_3 derived reagents). However, Dess−Martin oxidation was successful. The initial product was the 4-*endo*-phenylbicyclic stereoisomer, which was identified by NMR analysis and epimerized directly to afford the desired 4-*exo*-diastereomer **14** as depicted in Scheme 3.

The stereochemical assignments were from NMR analysis and are given in the Experimental Section. The case of alcohol **13** was especially critical and an assignment of the phenyl group at C4 as *endo* was based on a comparison of HC4−HC3 coupling constants with literature examples.[12]

(B) Solid-State Photolyses. (1) 2-Methyl-4,4-diphenylcyclohex-2-enone (9). Previously[2b,5] we have noted that solid-state photolysis of 2-methyl enone **9** affords not only the common Type B enone photoproduct **16**[13] but also the ring-contracted cyclopentenone **17**. Additionally, there was evidence that the product ratio was dependent on the extent of conversion. Thus, we planned to study the process more closely. The reaction proceeds in stages[2b] with products **16** and **17** being formed in a 1:1 ratio up to 10% conversion. At this point the exclusive photoproduct being formed becomes the bicyclic

(11) Frisch, M. J.; Trucks, G. W.; Schlegel, H. B.; Scuseria, G. E.; Robb, M. A.; Cheeseman, J. R.; Zakrzewski, V. G.; Montgomery, J. A., Jr.; Stratmann, R. E.; Burant, J. C.; Millam, J. M.; Daniels, A. D.; Kudin, K. N.; Strain, M. C.; Farkas, O.; Tomasi, J.; Barone, V.; Cossi, M.; Cammi, R.; Mennucci, B.; Pomelli, C.; Adamo, C.; Clifford, C.; Ochterski, J.; Petersson, G. A.; Ayala, P. Y.; Cui, Q.; Morokuma, K.; Malick, D. K.; Rabuck, A. D.; Raghavachari, K.; Foresman, J. B.; Cioslowski, J.; Ortiz, J. V.; Stefanov, B. B.; Liu, G.; Liashenko, A.; Piskorz, P.; Komaromi, I.; Gomperts, R.; Martin, R. L.; Fox, D. J.; Keith, T.; Al-Laham, M. A.; Peng, C. Y.; Nanayakkara, A.; Gonzalez, C.; Challacombe, M.; Gill, P. M. W.; Johnson, B.; Chen, W.; Wong, M. W.; Andres, J. L.; Gonzalez, C.; Head-Gordon, M.; Replogle, E. S.; Pople, J. A. *Gaussian 98*, Revision A.9; Gaussian, Inc.: Pittsburgh, PA, 1998.

(12) Rees, J. C.; Whittaker, D. *Org. Magn. Reson.* **1981**, *15*, 363−369.

(13) (a) Zimmerman, H. E.; Wilson, J. W. *J. Am. Chem. Soc.* **1964**, *86*, 4036−4042. (b) Zimmerman, H. E.; Rieke, R. D.; Scheffer, J. R. *J. Am. Chem. Soc.* **1967**, *89*, 2033−2047. (c) Zimmerman, H. E.; Kutateladze, A. G. *J. Org. Chem.* **1995**, *60*, 6008−6009.

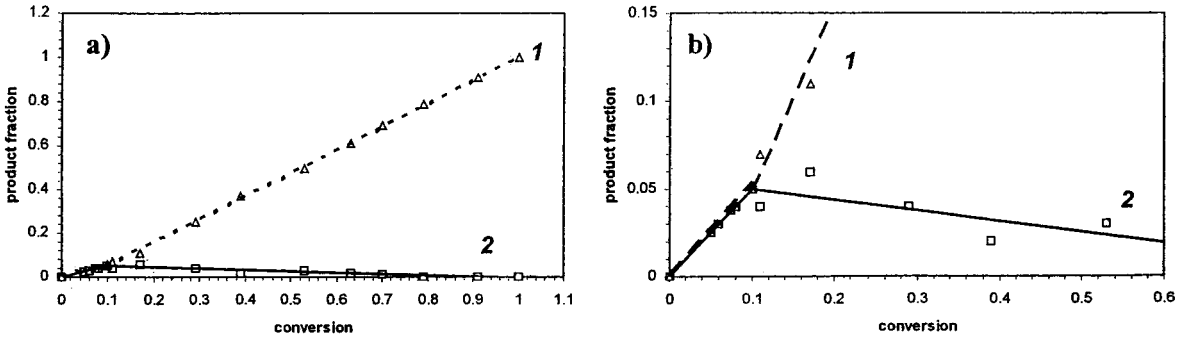

Figure 1. Stages and changes in reactivity with extent of conversion of reactant **9**. The expanded graph (b) shows the area in graph a corresponding to low conversions. Plot ***1*** corresponds to photoproduct **16**, plot ***2*** corresponds to **17**.

Scheme 4. Photochemistry of 2-Methyl-4,4-diphenylcyclohex-2-enone (**9**)

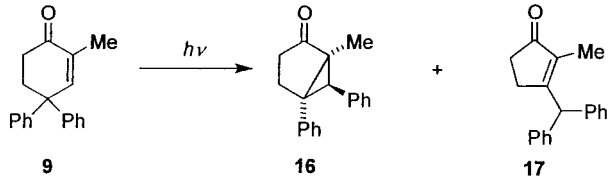

Solution:	1.0	0
Solid-state stage 1 (to 10%):	1.0	1.0
Solid-state stage 2 (above 10%):	1.0	0

Scheme 5. Two Alternative Labeling Results

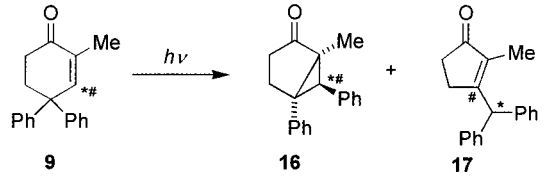

Label # if by direct ring contraction
Label * if via bicyclic **16** and a secondary rearrangement

ketone **16**. Cyclopentenone **17** formed from stage 1 remained except for a slow loss due to secondary conversion[5] to bicyclic **16**. The process finally leads to its total disappearance at the end of stage 2. Scheme 4 gives these results, and the stage behavior is shown in Figure 1 and summarized in the table in Scheme 4 that gives *incremental* amounts of formation of the products in the two stages. The zero value for **17** in stage 2 might well have been given a negative incremental value but does clarify that this isomer is not being formed.

The unusual formation of the five-membered-ring product **17** had little precedent in the photochemistry of 4,4-diaryl-substituted cyclohexenones. One can consider two, alternative mechanisms. One involves direct ring-contraction and the other involves a secondary reaction to be discussed (vide infra). By use of the ^{13}C-labeled reactant it was possible to differentiate between the possibilities. The two labeling alternatives are shown in Scheme 5 with the differing dispositions of the originally labeled β-carbon in the products. Experimentally, the NMR spectrum of the photoproduct **17** showed that the ^{13}C resulted at the benzhydryl carbon (i.e. label with an asterisk in Scheme 5), thus precluding the simple ring contraction alternative (vide infra).

One further interesting point is that bicyclic ketone **16** turned out to be unreactive in solution (note eq 1), although 5,6-diphenyl bicyclic ketones, lacking the 2-methyl group, are known to undergo *cis*−*trans* isomerization.[14]

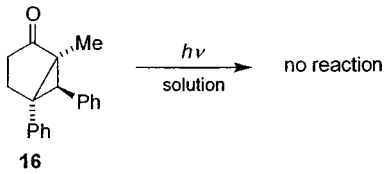

(1)

(2) 4,5,5-Triphenylcyclohexenone (18). In previous studies[15] we investigated the solution photochemistry of 4,5,5-triphenylcyclohexenone (**18**). The corresponding behavior in the crystal lattice proved quite different and particularly interesting. Both reaction courses are illustrated in Scheme 6 along with details of the stage behavior that was once again encountered. Hence, the main products in solution were stereoisomeric cyclobutanones **19** and the *exo* stereoisomer of bicyclic ketone **20**. The solid-state products differed completely. The bicyclic ketone **14** resulted from an unusual and novel rearrangement, termed Type C. Also the *endo* stereoisomer **21**, a product of the Type B rearrangement, was formed. We note here the complete reversal of the 6-*exo*-phenyl stereochemistry characteristic of the solution photochemistry.

This example is particularly striking in giving a complete change of products in the second reaction stage. Thus in stage 1 photoproduct **14** was formed exclusively while in stage 2 bicyclic ketone **21** resulted as the major product. Again, the stage behavior had an early onset, at 12%. Note Figure 2. Ketone **21** is still another example of a product available synthetically only in the second stage of a multistage reaction.

One additional observation is of importance. At 12% conversion stage 1 ends and stage 2 begins. However, at close to one-half of this conversion the quantum yield drops sharply. This could be termed the existence of stage 1a and stage 1b, namely a crystal lattice change within stage 1. This is depicted in Figure 3. We know that there is some change in the environment of the reactant at the end of stage 1a to account for the drop in quantum yield. The simplest assumption is the formation of one product **14** as a neighbor at this point. This means, from the quantum yield behavior in Figure 3, that at the end of stage 1, there must be two neighboring molecules of **14**.

(3) 3-*tert*-Butyl-5,5-diphenylcyclohexenone (4). Interestingly, *tert*-butyl enone **4** behaved quite differently than the

(14) Zimmerman, H. E.; Hancock, K. G.; Licke, G. *J. Am. Chem. Soc.* **1968**, *90*, 4892−4911.
(15) Zimmerman, H. E.; Solomon, R. D. *J. Am. Chem. Soc.* **1986**, *108*, 6276−6289.

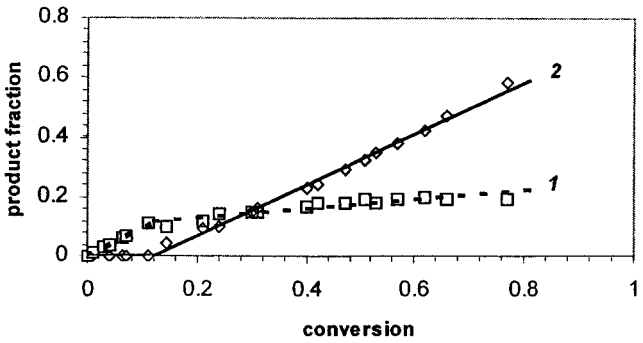

Figure 2. Stages and changes in reactivity with the extent of conversion of reactant **18**. Plot ***1*** corresponds to photoproduct **14**, plot ***2*** corresponds to photoproduct **21**.

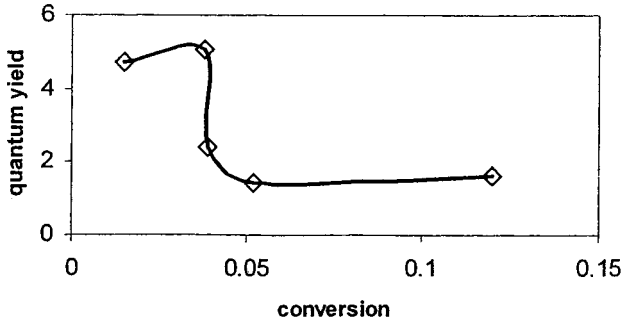

Figure 3. Conversion dependence of solid-state quantum yield for 4,4,5-triphenylcyclohex-2-enone (**18**). The values of quantum yield are multiplied by 10^4.

Scheme 6. Solution and Solid-State Photochemistry of 4,5,5-Triphenylcyclohex-2-enone (**18**)

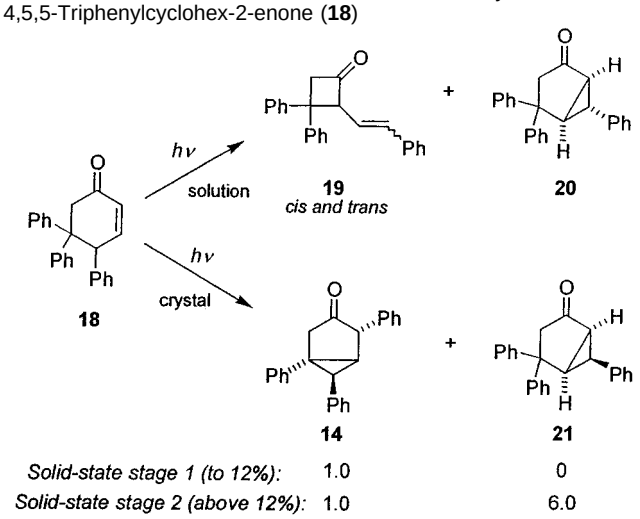

ftriphenyl enone **18**, which gave the Type C δ to α migration only in the crystal lattice but afforded the Type B product in solution. The solution photolysis of **4** led to three photoproducts: two isomeric bicyclic ketones, **22** and **23**, and cyclohexenone **24**. We note that all three photoproducts arose from a Type C transformation.

The solid-state photolysis of enone **4** also exhibited the Type C reactivity, but in contrast to the solution behavior, selective formation of a single Type C photoproduct **23** was encountered, and this persisted to 67% conversion. Beyond this limiting conversion, crystal melting precluded a search for a stage 2 reaction. Also the solid-state reaction proved quite efficient

Scheme 7. Solution Photochemistry of *tert*-butyl Enone **4**

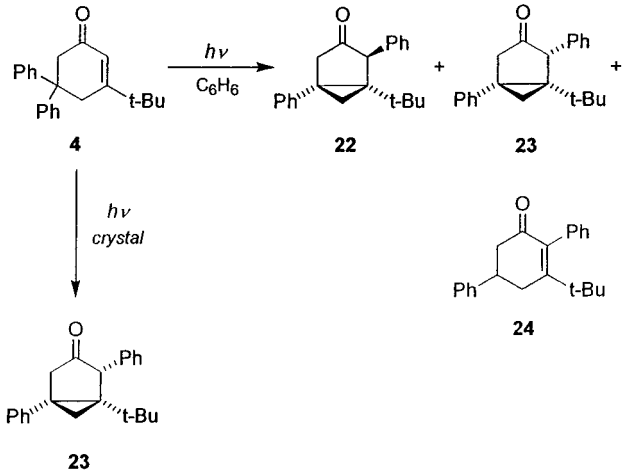

with a quantum yield of 0.017. This chemistry is shown in Scheme 7.

(C) Computations. Our theoretical approaches have been based on our "mini-crystal lattice concept" which permits quantitative description of the reaction cavity and of the behavior of the reacting species within this cavity. Such a modeling of the solid-state reaction is of importance since in many cases it is the only possible method to get a reasonable answer to why a reaction occurs in a given way. The mini-crystal lattice is derived from the X-ray data for the reactant by using a special computer program.[5b] It is composed of a central molecule surrounded by a sufficient number of the neighboring molecules building the reaction cavity. Then the central molecule is computationally transformed to a molecule representing a transition state of the reaction followed by molecular mechanics and then ONIOM optimization of this transition structure inside the reaction cavity. This produces the geometry and energy of this species, which can be directly compared with those for the alternative species and reaction pathways.

The method allows ab initio optimization of reacting species inside a two-layered minicrystal lattice that is treated by molecular mechanics. The first layer is composed of the closest surrounding molecules (5−25 molecules) and represents a reaction cavity. All the other more distant molecules of the mini-lattice are included in the second layer. The first layer is allowed to optimize, while the second layer is kept frozen during the entire optimization. An optimization of the reacting cavity together with the reacting species allows removal of stress imposed on the reacting central molecule by the reaction cavity (i.e. crystal pressure).[16] More details of the computational method may be found in the Experimental Section.

(1) 2-Methyl-4,4-diphenylcyclohex-2-enone (9). In the case of the unusual stage photochemistry of 2-methyl-4,4-diphenylcyclohex-2-enone (**9**), we turned to computational modeling at various points in the reaction course. A first problem was to analyze why an originally formed bicyclic product **16** undergoes such an unusual transformation to cyclopentenone **17**. To this end, a molecule of bicyclic triplet **16T** was optimized inside a mini-lattice consisting of ground-state neighbors. Then this triplet ($\mathbf{16T_{cr}}$) was compared with the same triplet ($\mathbf{16T_{gas}}$) optimized as a single molecule (i.e. gas phase). The ab initio

(16) McBride, J. M. *Acc. Chem. Res.* **1983**, *16*, 304−312.

Table 1. Comparison of Energies of Bicyclic Triplets **16T**[a]

	ab initio energy, au[b]	ΔE, kcal/mol[b]
16T$_{gas}$, optimized in gas phase	−804.7447991	0
16T$_{cr}$, optimized in crystal	−804.6830413	38.8
16T$_{cr}$′, optimized in crystal[c]	−804.6909315	33.8

[a] Geometries were optimized with HF/6-31G* for the gas phase and with ONIOM (HF/6-31G*: Dreiding) for the enone crystal. [b] HF/6-31G*, note energy differences of over 0.5 kcal/mol are significant. [c] Formed from the second reacting molecule in the surrounding shell of enone molecules but with the one adjacent enone converted to cyclopentenone **17**.

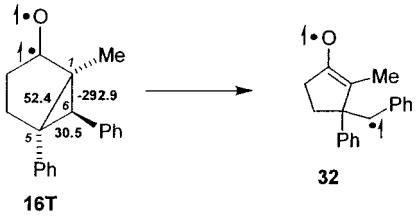

Figure 4. Results of the Delta-Density analysis of the bicyclic triplet **16T** and suggested bond 1−6 fission to form biradical **32**. Numbering in the three-membered ring is shown in *italics*, ΔD changes are given in **bold** print.

energies of both species are given in Table 1, where we note the triplet **16T$_{cr}$** to be 38.8 kcal/mol higher in energy than its gas-phase counterpart. The importance of these relative energies is considered in the Discussion section below.

Additionally, there is a striking difference in geometry relative to **16T$_{gas}$**. The C6 to *ipso*(phenyl) bond of **16T$_{cr}$** is bent from normal with a distortion angle 11° and seems responsible for the much higher energy of this intermediate. Interestingly, almost the same distortion was obtained in the preliminary molecular mechanics optimization, indicating that the distortion mainly results from intermolecular steric repulsion. The last species, **16T$_{cr}$**′, in Table 1 is a neighbor to **16T$_{cr}$**, which is converted to cyclopentenone product.

A quantitative analysis of the distribution of bond distortions was obtained from our Delta Density analysis.[17] This method compares the density matrices for two species as in eq 2. In the present instance, the two species of interest are the relaxed, gas-phase enone triplet **16T$_{gas}$** and the triplet **16T$_{cr}$** as formed in the crystal lattice. The basis orbitals used are the Weinhold NHO's.[18] Positive elements correspond to strengthened bonds in **16T$_{cr}$** relative to **16T$_{gas}$** while negative elements correspond to weakened bonds. This analysis revealed that the C1−C6 bond of the bicyclic triplet **16T$_{cr}$** is markedly weakened (by 0.3 electrons) as illustrated in Figure 4, which gives ΔD values for bonds of interest. This accounts for the high reactivity of **16** in stage 1 in proceeding onward to form **17**.

$$\overline{\overline{\Delta \mathbf{D}}} = \overline{\mathbf{D}}_{\mathbf{cr}} - \overline{\mathbf{D}}_{\mathbf{gas}} \qquad (2)$$

To understand the product distribution in the reaction of enone **9** it seemed necessary to evaluate the structure and energy of the half-migrated species **25T** leading from the triplet of enone **9** onward to photoproduct **16**. The energetic results of these computations are given in Table 2.

Table 2. Ab Initio Energies for Triplet Intermediates **25T**[a]

	ab initio energy, au[b]	ΔE, kcal/mol
25T$_{gas}$, optimized in gas phase	−804.7344249	0
25T$_{cr}$, optimized in crystal	−804.6929934	26.0
25T$_{cr}$′, optimized in crystal[c]	−804.7160792	11.5

[a] Geometries were optimized with HF/6-31G* for the gas phase and with ONIOM (HF/6-31G*: Dreiding) for the crystal. [b] HF/6-31G*. [c] Formed from the second reacting molecule in the surrounding shell.

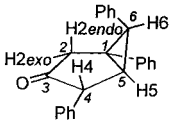

^{13}C chemical shifts			^{1}H chemical shifts		
atom	δ calcd, ppm	δ exp., ppm	atom	δ calcd, ppm	δ exp., ppm
C1	36.8	32.5	H2*exo*	2.9	3.06
C2	40.0	41.5	H2*endo*	2.6	2.80
C3	203.8	212.7	H4	3.7	3.70
C4	57.8	55.6	H5	2.6	2.80
C5	36.2	32.0	H6	2.7	2.88
C6	42.8	35.4			

Figure 5. Calculated (GIAO RHF/6-31G(df,pd)//B3LYP/6-31G(d,p)) versus experimental NMR chemical shifts for photoproduct **17**.

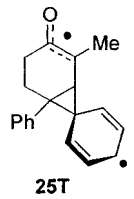

25T

(2) 4,5,5-Triphenylcyclohexenone (18). The conversion of triphenyl enone **18** in the solid state to the bicyclic product **14** involves a novel transannular δ to α phenyl migration as noted earlier. As a check on the structure assignment, it seemed prudent to obtain the theoretical ^{13}C and ^{1}H NMR chemical shifts for this photoproduct. This was done by using GIAO computations, as available in Gaussian 98. The values are listed in the Figure 5. The agreement with experiment is quite good.

A second item concerned the photochemistry. To understand the reaction mechanism proceeding via an unusual δ to α phenyl migration, which we term a Type C rearrangement, ab initio computation of species along the mechanistic pathway proved helpful. Similarly, we followed the pathway of the Type B rearrangement of triphenyl enone **18**; however, in this case, our computations included only species **26T** and **27T** and the transition structure between them. Energies of the intermediate species of interest as obtained computationally with Hartree−Fock UHF/6-31G* geometry optimization are summarized in Table 3. These results led to the question of whether the two reactions proceed via different reactant triplets of enone **18**, with these triplets differing not only in energy and electronic configuration but also in geometry. Indeed this was the case. Table 3 includes energies for triplets **26T** (planar) and **29T**

(17) (a) Zimmerman, H. E.; Alabugin, I. V. *J. Am. Chem. Soc.* **2001**, *123*, 2265−2270. (b) Zimmerman, H. E.; Alabugin, I. V. *J. Am. Chem. Soc.* **2000**, *122*, 952−953.
(18) (a) Foster, J. P.; Weinhold, F. *J. Am. Chem. Soc.* **1980**, *102*, 7211−7218. (b) Reed, A.; Curtiss, L. A.; Weinhold, F. *Chem. Rev.* **1988**, *88*, 899−926.

Scheme 8. Mechanisms of Type B versus Type C Enone Rearrangements for Enone **18**

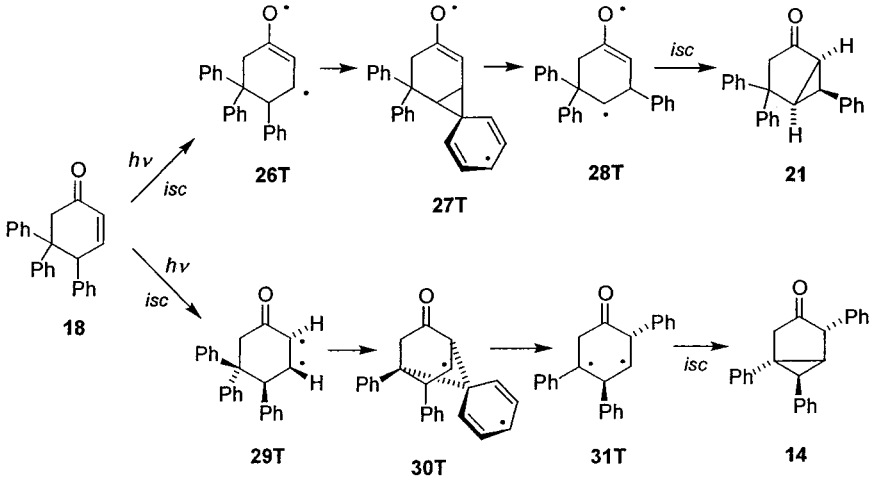

Table 3. Energies of the Intermediate Species Included in the Photochemistry of Enone **18**

reaction species[a]	ab initio energy, au[b]	rel energy, kcal/mol[b]
A, S0 of enone **18**, relaxed geometry	−995.3351504	0.7
B, $\pi-\pi^*$ twisted triplet **29T**	−995.2492053	54.6
C, TS **29T** → **30T**	−995.2005462	85.2
D, half-migrated triplet intermediate **30T**	−995.2359950	62.9
E, triplet biradical **31T**	−995.2804044	35.1
F, bicyclic product **14**, S0	−995.3361895	0
G, n−π^* planar triplet **26T**	−995.2684720	42.5
H, TS **26T** → **27T**	−995.2419138	59.2
I, half-migrated triplet intermediate **27T**	−995.2581979	49.0

[a] Geometry was optimized with the HF/6-31G* level. [b] HF/6-31G*.

Table 4. Delta Density Computation Results for the Two Excited States of the Triphenyl Enone **18**[a,b]

orbitals	planar triplet **26T**	twisted triplet **29T**
π C=C	−1174.9	−4483.8
π C=O	−2391.8	−1420.9
n_y	−9146.0	−866.0

[a] UHF/6-31G*. [b] Versus ground-state S0 as a reference point.

Table 5. CASSCF/NBO Analysis of the Electronic Configuration of the Triplets **26T** and **29T**[a,b]

	electronic population[c]	
orbitals	planar triplet **26T**	twisted triplet **29T**
π_2^*	0.4198	0.2230
π_1^*	1.0141	0.9235
n	1.0073	1.9238
π_2	1.6568	0.9853
π_1	1.8929	1.8643

[a] Geometries were optimized with CASSCF(6,5)/6-31G* with the NBO basis set. [b] CASSCF energies: for **26T** −995.2822647 au, for **29T** −995.2796512 au. [c] In electrons.

(twisted). These were obtained as local energy minima by starting the optimization, in one case (**26T**), with the ground-state enone **18** and, the other (**29T**), from the search for the transition structure between **26T** and **30T**. Both pathways are outlined in Scheme 8. This is further considered in the Discussion section.

To establish the electronic structure of these triplets, we used our Delta-Density analysis and also CASSCF/NBO computations.[19] These computational results on triplets **26T** and **29T**, planar and twisted, are given in Tables 4 and 5.

Table 6. Comparison of Energies of Reacting Intermediates for Two Competing Pathways in Different Media[a]

	Type B migration (intermediate **27T**)		Type C migration (intermediate **30T**)	
	ab initio energy, au[b]	rel energy, kcal/mol[b]	ab initio energy, au[b]	rel energy, kcal/mol[b]
gas phase	−995.2581979	0	−995.2359950	0
crystal	−995.1830517	47.2	−995.2243063	7.3
crystal, stage 2[c]	−995.2083939	31.3	−995.2050612	19.4

[a] Geometries were optimized with HF/6-31G* for the gas phase and with ONIOM (HF/6-31G*: Dreiding) for the crystal. [b] HF/6-31G*. [c] Molecule reacting in stage 2, optimized in the crystal together with two molecules of product **14** (see the Discussion Section).

Table 7. Energies of Ground and Triplet States of *tert*-Butyl Enone **4**

reaction species[a]	ab initio energy, au[b]	rel energy, kcal/mol[b]
ground state, relaxed geometry	−921.9353821	0
$\pi-\pi^*$ twisted triplet	−921.8662925	43.4
n-π^* planar triplet	−921.8450080	56.7

[a] Geometry was optimized with the HF/6-31G* level. [b] HF/6-31G*.

Computations were also carried out for the reaction intermediates **27T** and **30T** in the mini-crystal lattice of triphenylenone **18** obtained from the X-ray coordinates. This was done with ONIOM. The results are given in Table 6.

(3) 3-*tert*-Butyl-5,5-diphenylcyclohexenone (4). With relatively close energies for both the twisted and planar triplet states of the triphenylenone **18**, we proceeded to look at the 3-*tert*-butyl-5,5-diphenylcyclohexenone (**4**) excited states. The energies obtained are given in Table 7.

To search for a source of the high efficiency and selectivity in the crystalline state reaction of this enone, an ONIOM computation in the mini-crystal lattice was carried out for the half-migrated triplet counterpart of **30T**. Also computations were carried out on the two alternative ground-state products **22** and **23**. These results are shown in Table 8. The interpretation of these results is given in the Discussion section.

Discussion

The Mechanism of Formation of Cyclopentenone 17. It has been noted above and in Scheme 5 that two alternative

(19) Nemukhin, A. V.; Weinhold, F. *J. Chem. Phys.* **1992**, *97*, 1095−1108.

Table 8. Computational Results for the Enone **4** Type C Rearrangement Species[a]

	ab initio energy, au	ΔE, kcal/mol[b]
half-migrated intermediate optimized in the gas phase	−921.8353739	0
half-migrated intermediate optimized in the crystal	−921.8289199	4.1
photoproduct **23** optimized in the crystal	−921.8465375	0
photoproduct **22** optimized in the crystal	−921.8224607	15.1

[a] Geometries were optimized with HF/6-31G* for the gas phase and with ONIOM (HF/6-31G*:Dreiding) for the crystal. [b] Comparison between lines 1−2 and 3−4, respectively.

Scheme 9 The Mechanism of Formation of **17** According to the Labeling Experiment

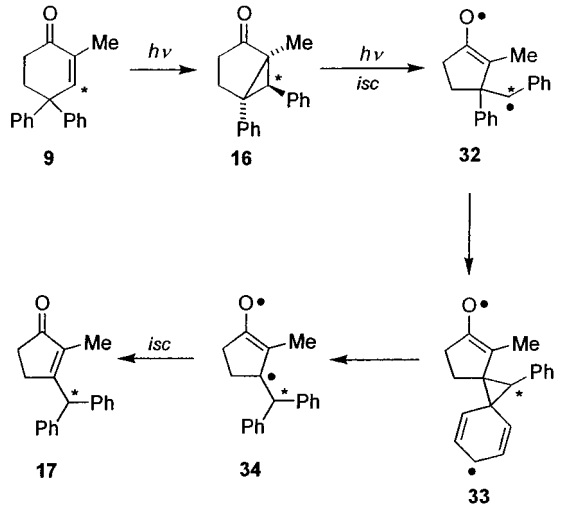

Scheme 10. Understanding of Constancy of the **16** to **17** Ratio in Stage 1

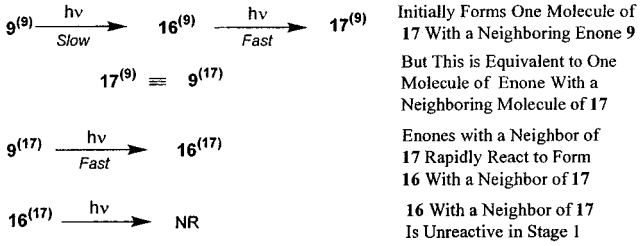

mechanisms were considered for the formation of photoproduct **17** that was formed in the solid-state photolysis in stage 1; see Scheme 1. The direct ring contraction mechanism is certainly the simplest and was initially favored. However, this mechanism would leave the ^{13}C label at the β carbon of the cyclopentenone ring as outlined in Scheme 5 and not at the benzhydryl site. Clearly the product arises from the mechanism outlined in Scheme 9, which depicts an initial Type B phenyl migration followed by a reaction of the initially formed bicyclic photoproduct **16**. Opening of the three-membered ring in this manner as noted has precedent in *cis*−*trans* stereoisomerization of bicyclo[3.1.0]hexanones.[14] In this case triplet diradical **32** undergoes a phenyl migration with concomitant intersystem crossing to afford the photoproduct **17** with the experimentally observed labeling.

One further point is the contrast between two findings: (a) the sequential mechanism of conversion of **9** to **16** to **17** as required by the labeling evidence and (b) the constant 1:1 ratio of **16** to **17** during stage 1 that forms **16** and **17**. Our interpretation is outlined in Scheme 10. Here molecule pairs are represented as "**MOLECULE**$^{\textbf{(Neighbor)}}$". Every molecule of **16** formed in stage 1 (we term this **16**$^{(9)}$) has a closest neighbor enone **9** molecule adjacent. Each of these molecules **16**$^{(9)}$ proceeds to form a molecule of **17** that then also has an enone neighbor (i.e. termed **17**$^{(9)}$ or **9**$^{(17)}$) which, in turn, is strongly perturbed and is triggered to a very fast reaction of this enone molecule **9**$^{(17)}$ leading quickly to another molecule of **16** with a neighbor of **17**. Hence the process uses two enone molecules to form one molecule of **16** and one of **17**, and the ratio remains 1:1 overall.

Thus **16**$^{(9)}$ and **9**$^{(17)}$ are postulated to be particularly reactive while bicyclic molecules with a cyclopentenone product **17** neighbor (i.e. **16**$^{(17)}$) are postulated to be unreactive. This is a unique requirement for 1:1 formation of **16** and **17** in stage 1 of the reaction.

The high reactivity of **16**$^{(9)}$ in the crystal cavity for bond 1−6 fission compared with the lack of reactivity in solution is understood from Delta-Density considerations. Thus, as noted in the section on Computational Results, a Delta Density analysis of the bicyclic ketone triplet **16T**$_{cr}$, geometry optimized within the mini-crystal lattice composed of enone reactant, and compared with its optimized gas-phase counterpart **16T**$_{gas}$, revealed bond 1−6 to have a large negative matrix element and thus to be selectively weakened. Note Figure 4. It is this bond that is opened in the mechanism leading to photoproduct **17** as outlined in Scheme 9. Thus, bond 1−6 weakening arises from distortion of the phenyl group attached to C6 by the cavity.

The computational data in Tables 1 and 2 also are in accord with the experimentally observed reactivity presented above. Interestingly, even before use of quantum mechanical optimization, molecular mechanics optimization revealed that the bicyclic triplet **16T**$_{cr}$ formed inside the crystal cavity is of much higher energy than its gas-phase analogue **16T**$_{gas}$. An ab initio difference of 38.8 kcal/mol was found. The energy of **16T**$_{cr}$, corresponding to **16**$^{(9)}$ in Scheme 10, is higher than the energy of **16T**$_{cr}'$, which corresponds to **16**$^{(17)}$ in this scheme (note Table 1). This suggests a higher reactivity for the initially formed **16** compared with the second molecule of **16** produced. Also, this is consistent with the lack of reactivity of **16**$^{(17)}$. Table 2 gives information about the "half-migrated" triplet species **25T** of the two processes of interest. In this table **25T**$_{cr}$, corresponding to the bridged species leading from **9** to **16**$^{(9)}$, is of considerably higher energy than **25T**$_{cr}'$, which is the bridged intermediate formed from **9**$^{(17)}$ affording **16**$^{(17)}$. Thus **9**$^{(9)}$ is much less reactive compared with **9**$^{(17)}$. The net theoretical conclusion is that the initial enone reaction occurs somewhat more slowly than the subsequent reaction of a second molecule of the reaction cluster.

A further point concerns stage 2. It is seen that the energies of the half-migrated intermediates of the surrounding unreacted enone molecules at the beginning of stage 2 are in the range of 25−27 kcal/mol as determined by MM3 computation. This compares with that for the initial central molecule of stage 1 (i.e. **25T**$_{cr}$) where the energy is 26.9 kcal/mol. Hence these species do not react competitively with the two molecules of stage 1, but react only slowly at stage 2.

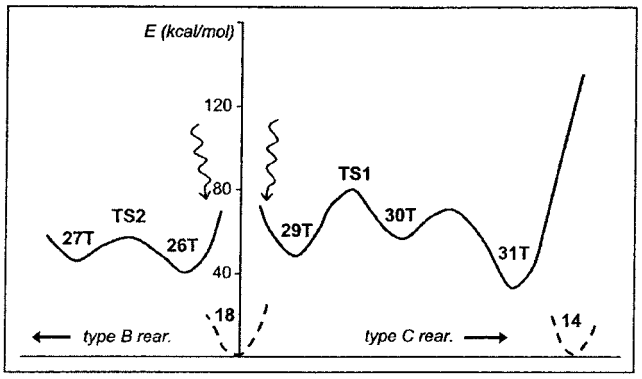

Figure 6. Schematic representation of the reaction path for the photochemical rearrangements of 4,5,5-triphenylcyclohex-2-enone (**18**). The dashed line corresponds to S0 and the solid lines correspond to two different T1 states.

There is another point requiring comment concerning our use of molecular mechanics for this computation. It is clear that molecular mechanics does not afford good absolute accuracy as electronic (e.g. delocalization) effects are neglected. But since the main source of intermolecular interactions in these systems comes from steric repulsions, for comparative purposes, molecular mechanics with the MM3 force field is reliable.

The Mechanism of the Reaction of 4,5,5-Triphenylcyclohexenone (18). The first item requiring attention is the unusual course of the solid-state rearrangement of the triphenylenone **18**. As outlined in Scheme 6, the known solution reaction[15] leads to the usual Type B bicyclohexanone product **20** and, with ring-contraction, to vinylcyclobutanones **19**. In contrast, in stage 1 of the solid-state reaction the exclusive formation of triphenyl bicyclic **14**, termed a Type C rearrangement, involves a δ to α migration.

The preference for the Type B rearrangement in solution, rather than the Type C, can be understood from inspection of the data in Table 3. Thus, the half-migrated intermediate **27T** of the Type B reaction is 13.9 kcal/mol lower in energy than the corresponding **30T** of the Type C process.

Moreover, a comparison of the alternative transition states **TS1** and **TS2** (note Figure 6) shows a preference of 26.0 kcal/mol for the Type B rearrangement. We also see that the calculated activation energy of 16.7 kcal/mol obtained for the triplet Type B rearrangement as the difference between entries *H* and *G* of Table 3 (**TS2** and **26T** in Figure 6) is in good agreement with the experimental value of 10−11 kcal/mol for the reaction in solution.[20]

However, for the crystal reaction, ONIOM computations for the same half-migrated species imbedded in the usual reactant mini-crystal lattice make clear the preference for this unusual reaction in stage 1. Thus, it is seen that the energy of the δ to α (Type C) migration is preferred over the common Type B process by 7.3 kcal/mol.

Additionally, as noted, the computations reveal that the Type C rearrangement is characteristic of the $\pi-\pi^*$ twisted triplet. Thus, two energy minima were obtained for the triplet of enone **18**, these corresponding to structures **26T** and **29T**. The former, **26T**, had a nearly planar enone moiety (i.e. $O-C_\alpha-C_\beta-C_\gamma$ dihedral angle of 0.5°). However, **29T** had the π-bond strongly twisted with a dihedral angle of 35°. We note in that, of the two enone triplets, **29T** is of higher energy by 12.1 kcal/mol (note Table 3). The Delta Density computations reveal that the triplet **26T** had lost almost 10 times the p_y orbital density compared with the twisted triplet **29T**. Also, it had lost much more π-bond density from the carbonyl. This identifies triplet **26T** as $n-\pi^*$. In contrast, the triplet **29T** had lost electron density mainly from the α,β-carbon bond, which identifies it as $\pi-\pi^*$.

The CASSCF/NBO computations[19] using NBO's as a basis and an active space of (6,5) aimed at confirming the assignment of these triplets. The active space was taken to include only those eigenfunctions heavily participating in the excitation process. Thus, the active space was comprised of four butadiene-like orbitals and an oxygen lone pair (i.e. n or p_y) orbital. This permitted efficient computation, and the results are given in Table 5. Triplet **26T** is seen again to involve lone pair electron excitation ($n-\pi^*$) while for triplet **29T** a $\pi-\pi^*$ configuration is dominant.

Turning to the stage phenomenon, from the quantum yield versus conversion measurements (note Figure 3), we can see that stage 2 does not begin until two molecules of reactant have undergone stage 1 reaction. Thus, the quantum yield drops precipitously after every reactant molecule has one molecule of photoproduct as a neighbor. The second ONIOM computation was carried out with the two neighbors of the central reactant molecule replaced by photoproduct **14** molecules. The choice of the neighbors had been taken at the locus where the Type C rearrangement resulted in maximum geometric change and thus maximum cavity shape modification. The result of this computation is the third entry in Table 6. Here it is seen that there is a predicted preference for the Type B rearrangement in stage 2. Moreover, the energetic preference of 2.1 kcal/mol over the Type C pathway corresponds approximately to the observed selectivity in stage 2 of 6:1.

The Mechanism of the 3-*tert*-Butyl-5,5-diphenylcyclohexenone 4 Reaction. It was originally computationally predicted that the Type C rearrangement originates from the $\pi-\pi^*$ triplet rather than the $n-\pi^*$ triplet. The latter commonly affords the Type B rearrangement. The Type C rearrangement of the *tert*-butylcyclohexenone **4** was of particular interest because it occurred even in solution. Here, even without a crystal environment, geometry optimization (gas phase) led to a twisted triplet (note Table 7) that is lower in energy. The corresponding planar triplet proved to be 13.3 kcal/mol higher in energy as a consequence of the steric effect of the *tert*-butyl group in facilitating π-bond twisting. Thus, the more stable twisted $\pi-\pi^*$ triplet led to the solution Type C rearrangement in this case.

Two important points are worth discussing. The first is the high efficiency of the solid-state photoreaction of enone **4**. Extrapolated to zero conversion, quantum yield turned out to be 0.017, which is in the usual range of the quantum yields for many solution photorearrangements (e.g. the solution quantum yield for the Type B enone rearrangement was determined to be 0.043[21]). To explain this ease of crystalline Type C rearrangement, a half-migrated intermediate corresponding to the $\delta-\alpha$ phenyl migration for the enone **4** has been optimized with ONIOM inside the mini-crystal lattice. The results are given in Table 8. For comparison purposes an energy of the same

(20) Zimmerman, H. E.; Elser, W. R. *J. Am. Chem. Soc.* **1969**, *91*, 887−896.

(21) Zimmerman, H. E.; Hancock, K. G. *J. Am. Chem. Soc.* **1968**, *90*, 3749−3760.

species optimized in the gas phase is included. One can see that the in-crystal optimized intermediate is only 4.1 kcal/mol higher than the corresponding gas-phase species. This reflects a very close "fit" of the shape of the crystalline reaction cavity to the reacting intermediate, as well as a spatial "compactness" of the type C transition state. Both factors allow the reaction to occur in the solid state with almost the same efficiency as in the solution.

The second point deals with a very high selectivity of the solid-state reaction that affords only one product **23** as compared with the solution reaction where three isomeric type C photoproducts **22**−**24** form. Again, such a high selectivity of the crystalline reaction may be qualitatively explained by the good fit of the reaction cavity to the only product ketone **23**. To obtain a quantitative support for this statement, the ONIOM optimizations of two alternative isomers **22** and **23** inside the enone **4** mini-crystal lattice have been conducted. The results are included in Table 8. An energetic preference of 15.1 kcal/mol for product **23** versus **22** has been found that explains its exclusive formation.

The Role of Cluster Size and Relaxation Effects. The last subject for discussion is the role of the size of the "reaction cluster", i.e., the number of surrounding molecules, that affects the reaction of a central molecule and whose reactivity is affected by it. This cluster may be considered as a minimal independent reacting unit of which the entire crystal is composed. Clearly it will include all the closest neighbors which form the first surrounding shell. Yet it is certainly smaller than our mini-crystal lattice. As was shown in a previous paper,[8] molecules more remote from the central molecule than the nearest shell have a minor effect on the central molecule reactivity. Thus, the "reacting cluster" practically coincides with the first surrounding shell. In the present cases of 2-methyl enone **9** and triphenyl enone **18**, this shell includes 14 molecules, so one can anticipate the size of the "reacting cluster" to consist of 15−20 molecules. This explains qualitatively why the switch between two stages in both solid-state reactions occurs at 10−12% conversion. This corresponds to the point where 2 molecules of 15−20 have already reacted, and only a slower reaction of the others takes place.

Relation to Previous Studies and Final Conclusion

Solid-state photochemistry has long exhibited remarkable promise for synthetic purposes. When we began our efforts in 1985, solid-state organic chemistry already had a very large number of examples where the crystal photochemistry differed from that in solution.[22] A restriction was that understanding was limited and largely qualitative. Further, the reactions investigated most often involved minimal molecular reorganization. Some quantitative treatments focused on reactant geometry.

Most important, Cohen and Schmidt had proposed the concept of the cavity in which molecules reacted.[3] These researchers also proposed the idea of least motion,[3a] and this has been termed the Topochemical Principle. A quantitative postulate was that for [2+2] cycloadditions a distance of 4.2 Å or less between π bonds was required.[22] Thomas and Ramamurthy advanced a still more quantitative theory for [2+2] cycloadditions involving packing potentials in which an empirical van der Waals function is used to assess the energy of the molecular pair in the cavity.[23] Warshel studied an excimer using an early QM/MM method.[24] One elegant approach utilized the proximity of an individual functional group to its nearest neighbor as in pretty studies by Lahav and Scheffer.[25] A different approach involved calculation of cavity volumes in a pioneering study by Gavezzotti.[26] Local stress has been utilized in important studies by McBride.[16]

However, in essentially all of these studies, the methods relied on reactant characteristics in the crystal to understand its reactivity. Our approach has been to compare the reacting species in the lattice with the original reactant. This is analogous to ground-state solution chemistry where it is helpful to compare a transition state with reactant rather than considering the reactant alone.

In particular, our finding of the phenomenon of reaction stages has provided an additional chance for obtaining photoproducts which are otherwise inaccessible. While hitherto an early loss of original crystal lattice ordering had been considered a limitation, this now promises to reveal subsequent stages with novel reactivity. Finally, the brilliant, but qualitative, concept of Cohen and Schmidt in envisioning crystal cavities in which reactions occur is now replaced by a "quantitative cavity" in which the cavity is precisely defined with the consequence that reactivity in the cavity can be computationally analyzed.

Experimental Section

General Procedures. All reactions were performed under an atmosphere of dry nitrogen. Melting points were determined in open capillaries and are uncorrected. Column chromatography was performed on silica gel (Aldrich, 60 Å, 200−400 mesh, or Silica gel 60 Geduran 35−75 μm) mixed with Sylvania 2282 phosphor and slurry packed into quartz columns to allow monitoring with a hand-held UV lamp. All solvents were additionally purified and dried by standard techniques. ^{1}H and ^{13}C NMR spectra were recorded at 300 and 75 MHz respectively, and are reported in ppm downfield from tetramethylsilane.

Solution Photolyses. Solution photolyses were carried out in an immersion reactor with a water-cooled jacket using a 400 W medium-pressure mercury lamp equipped with a 5 mm filter of a circulating 0.4 M solution of $CuSO_4$ unless stated otherwise. All solutions were purged with deoxygenated nitrogen for 1 h both prior to and during photolysis.

General Procedure for Solid-State Photolysis. Irradiation of fine crystalline material was performed between two quartz slides (5.0 × 5.0 cm^2) using a water-cooled medium-pressure 400 W mercury lamp equipped with a 2 mm Pyrex filter. To prevent possible melting during photolysis the samples were cooled in an ice−water bath. Each sample contained 50−75 mg of reactant crystals. For time-dependent photolysis purposes 5 mg portions were taken at fixed times and the product ratios were determined using ^{1}H NMR.

4,4-Diphenylcyclohexene (2) was prepared according to the procedure of Zimmerman et al.[27] in 64% yield as colorless crystals, mp 61−63 °C (lit.[27] mp 65−66.5 °C).

5,5-Diphenylcyclohex-2-enone (3). To a stirred solution of 18.0 g (76.9 mmol) of 4,4-diphenylcyclohexene (**2**) in 600 mL of benzene

(22) Schmidt, G. M. J. *Solid State Photochemistry*; Ginsberg, D., Ed.; Verlag Chemie: New York, 1976.

(23) (a) Thomas, N. W.; Ramdas, S.; Thomas, J. M. *Proc. R. Soc. London A* **1985**, *400*, 219−227. (b) Murthy, G. S.; Arjunan, P.; Venkatesan, K.; Ramamurthy, V. *Tetrahedron* **1987**, *43*, 1225−1240.

(24) Warshel, A.; Shakked, Z. *J. Am. Chem. Soc.* **1975**, *97*, 5679−5684.

(25) (a) Chang, H. C.; Popovitz-Biro, R.; Lahav, M.; Leiserowitz, L. *J. Am. Chem. Soc.* **1987**, *109*, 3883−3893. (b) Ariel, S.; Askari, S. H.; Scheffer, J. R.; Trotter, J.; Wireko, F. *J. Am. Chem. Soc.* **1987**, *109*, 4623−4626.

(26) Gavezzotti, A. *J. Am. Chem. Soc.* **1983**, *105*, 5220−5225.

(27) Zimmerman, H. E.; Epling, G. A. *J. Am. Chem. Soc.* **1972**, *94*, 7806−7811.

were added Celite (50.0 g) and PDC (44.0 g, 117.0 mmol). The resulting mixture was cooled to 10 °C, and *tert*-butyl hydroperoxide (11.7 g of 90% solution in *t*-BuOH, 116.7 mmol) was added dropwise. The reaction mixture was stirred for 26 h at room temperature. Then it was filtered through a Celite pad, and the filter was thoroughly washed with ether. The filtrate was successively washed with 5% HCl and water and dried over Na_2SO_4. After rotary evaporating the solvents, an oily residue was separated by column chromatography on silica gel (column 47.0 × 4.0 cm^2, eluent ethyl acetate−hexane 1:5) to give the following fractions: (a) 8.6 g of starting material as a colorless oil, crystallizing upon standing, R_f 0.78; (b) 5.5 g (57% based on consumed starting material) of 4,4-diphenylcyclohex-2-enone (**1**) as a colorless solid, R_f 0.47, which was recrystallized from an ether−hexane mixture to give colorless prisms, mp 94−97 °C (lit.[28] mp 96−97 °C); (c) 2.0 g (21% based on consumed starting material) of 5,5-diphenylcyclohex-2-enone (**3**) as a colorless solid, R_f 0.33, which was recrystallized from hexane−CH_2Cl_2 mixture to give 1.9 g of colorless crystals, mp 104−105 °C (lit.[27] mp 110.5−112.5 °C). ^{1}H NMR ($CDCl_3$) δ 7.32−7.14 (m, 10H), 7.01 (dt, J_1 = 9.6 Hz, J_2 = 5.4 Hz, 1H), 6.04 (dt, J_1 = 9.6 Hz, J_2 = 1.8 Hz, 1H), 3.22 (s, 2H), 3.19 (dd, J_1 = 4.2 Hz, J_2 = 1.8 Hz, 2H).

3-*tert*-Butyl-5,5-diphenylcyclohex-2-enone (4). A solution of *t*-BuLi (9.5 mL of 1.7 M solution in pentane, 16.2 mmol) was added to a stirred suspension of 0.73 g (8.1 mmol) of CuCN in 35.0 mL of ether at 0 °C. The resulting mixture was stirred for 10 min, and a solution of 1.0 g (4.0 mmol) of 5,5-diphenylcyclohex-2-enone (**3**) in 40.0 mL of ether was added dropwise at 0 °C, followed by stirring at this temperature for 3 h. A solution of PhSeBr[29] was prepared by addition of Br_2 (1.42 g, 0.46 mL, 8.87 mmol) to a solution of 2.87 g (9.2 mmol) of diphenyldiselenide in 20.0 mL of ether at intensive agitation. This PhSeBr solution was added rapidly to the reaction mixture (this was accompanied by immediate decolorization). The resulting mixture was poured into 150 mL of 5% HCl and 150 mL of ether−pentane (1:1). The organic fraction was separated, washed with saturated $NaHCO_3$ solution and water, dried over Na_2SO_4, and concentrated in vacuo. The oily residue was dissolved in 100 mL of methanol, and 0.77 g (9.2 mmol) of $NaHCO_3$ in 15.0 mL of H_2O and 7.88 g (36.8 mmol) of $NaIO_4$ in 35.0 mL of H_2O were added. After the mixture was stirred at room temperature for 3.5 h, the resulting solution was poured into a mixture of 80 mL of saturated $NaHCO_3$ solution and 100 mL of ether−pentane (1:1). The organic layer was washed with water and concentrated NaCl solution, dried over Na_2SO_4, and concentrated in vacuo. The crude product was purified by column chromatography on silica gel (column 48.0 × 2.5 cm^2, eluent ethyl acetate−hexane 1:5), and a fraction with R_f 0.44 afforded 0.58 g of colorless oil, which was crystallized from pentane to give 0.47 g (38%) of **30** as colorless prisms, mp 102−104 °C. ^{1}H NMR ($CDCl_3$) δ 7.30−7.12 (m, 10H), 5.95 (t, J = 1.2 Hz, 1H), 3.19 (s, 2H), 3.09 (s, 2H), 1.05 (s, 9H). UV (benzene), nm: 334 (ϵ = 45). HRMS *m*/*e* 304.1813 (calcd for $C_{22}H_{24}O$ 304.1827).

2-^{13}C-1,1-Diphenylethylene (6). The Wittig reaction was performed following the general procedure of Corey et al.[30] DMSO (10.0 mL) was added to sodium hydride (0.27 g of 60% suspension in mineral oil, 6.6 mmol) previously washed with pentane to remove mineral oil, and the resulting mixture was stirred at 50 °C to give a clear solution (ca. 1 h). This was cooled in an ice−water bath, and a solution of 2.62 g (6.47 mmol) of ^{13}C-methyltriphenylphosphonium iodide in 15.0 mL of DMSO was added dropwise. The resulting dark-yellow solution was stirred at room temperature for 30 min followed by addition of a solution of 1.18 g (6.47 mmol) of benzophenone in 5.0 mL of DMSO. After the addition was complete, the reaction mixture was stirred for 24 h at room temperature. Then it was poured into 100 mL of water, the mixture of solid and liquid was shaken with 5 × 50 mL portions of pentane, which were decanted, combined together, washed with water, and dried over Na_2SO_4. After concentration in vacuo the residue was purified by column chromatography (silica gel, column 21.0 × 2.5 cm^2, eluent pentane) to afford 0.84 g (76%) of the product as a colorless oil. ^{1}H NMR ($CDCl_3$) δ 7.37−7.29 (m, 10H), 5.46 (d, J = 158.4 Hz).

1-^{13}C-2,2-Diphenylethanol (7). A solution of 0.67 g (3.7 mmol) of 2-^{13}C-1,1-diphenylethylene (**6**) in 10.0 mL of THF was treated with a solution of BH_3−THF complex (7.4 mL of 1.0 M solution in THF, 7.4 mmol) at ice-bath temperature. The reaction mixture was stirred for 4 h at room temperature, cooled in a water-ice bath, and carefully treated with 2.0 mL of a 10% solution of water in THF followed by addition of 12.0 mL of a 3.0 M aqueous solution of NaOH (37.0 mmol) and 10.0 mL of 30% H_2O_2 (96.2 mmol). The resulting mixture was stirred for 1.5 h at room temperature, poured into water, acidified with 10% HCl, and extracted with ether. The organic fraction was washed with water and dried over Na_2SO_4. Removal of solvents in vacuo afforded a colorless oil, which was crystallized from hexane to give 0.57 g (74%) of the product as colorless cotton-like crystals, mp 51−52 °C. ^{1}H NMR ($CDCl_3$) δ 7.39−7.15 (m, 10H), 4.22 (dd, J_1 = 14.1 Hz, J_2 = 6.9 Hz, 1H), 4.18 (dt, J_1 = 143.7 Hz, J_2 = 7.2 Hz, 2H), 1.51−1.42 (m, 1H).

1-^{13}C-2,2-Diphenylacetaldehyde (8). A solution of 0.23 g (1.8 mmol) of oxalyl chloride in 5.0 mL of methylene chloride cooled to −70 °C was treated with a solution of 0.29 g (3.7 mmol) of DMSO in 1.0 mL of CH_2Cl_2.[31] The reaction mixture was stirred for 2 min, and a solution of 0.33 g (1.7 mmol) of 1-^{13}C-2,2-diphenylethanol (**7**) in 1.0 mL of CH_2Cl_2 was added via syringe. The resulting mixture was stirred for 20 min, and triethylamine (0.84 g, 8.3 mmol) was added dropwise followed by the stirring at −70 °C for an additional 10 min. Then the reaction mixture was allowed to warm slowly and stirred for 40 min at room temperature. It was diluted with CH_2Cl_2, washed successively with 3% HCl, water, saturated aqueous $NaHCO_3$, and water, dried over Na_2SO_4, and concentrated in vacuo. The crude product was purified by column chromatography (silica gel, column 35.0 × 1.5 cm^2, eluent ethyl acetate−hexane 1:5), the fraction with R_f 0.55 was collected, which afforded 0.25 g (76%) of the product as a colorless oil. ^{1}H NMR ($CDCl_3$) δ 9.89 (dd, J_1 = 178.5 Hz, J_2 = 2.6 Hz, 1H), 7.42−7.19 (m, 10H), 4.89 (dd, J_1 = 7.8 Hz, J_2 = 2.6 Hz, 1H).

3-^{13}C-2-Methyl-4,4-diphenylcyclohex-2-enone (*^{13}C*-9). A solution of KOH (0.15 mL of a 1.0 M solution in EtOH, 0.15 mmol) was added dropwise at 0 °C to the stirred solution of 0.17 g (0.86 mmol) of 1-^{13}C-2,2-diphenylacetaldehyde (**8**) and 80 mg (0.95 mmol) of ethyl vinyl ketone in 10.0 mL of anhydrous ether. The reaction mixture was stirred at 0 °C for 2 h followed by stirring at room temperature for 12 h. It was successively washed with 10% HCl, water, a concentrated solution of $NaHCO_3$, and water and dried over Na_2SO_4. After being concentrated in vacuo the oily residue was dissolved in 5.0 mL of ethanol, 1.0 mL of concentrated HCl was added, and the resulting mixture was stirred for 30 min at 60 °C. Then it was allowed to cool to room temperature, poured into water, extracted with ether, washed with concentrated $NaHCO_3$ and water, dried over Na_2SO_4, and concentrated in vacuo to afford a yellowish solid. This was recrystallized from methanol to give 0.15 g (65%) of colorless crystals, mp 116−118 °C. ^{1}H NMR ($CDCl_3$) δ 7.37 (m, 10.5 H), 6.80 (br. s, right part of =^{13}CH doublet, 0.5H), 2.72−2.63 (m, 2H), 2.41 (dd, J_1 = 7.0 Hz, J_2 = 5.5 Hz, 2H), 1.92 (dd, J_1 = 6.0 Hz, J_2 = 1.5 Hz, 3H). HRMS *m*/*e* 263.1383 (calcd for ^{13}C $C_{18}H_{18}O$ 263.1391).

***trans*-5,6-Diphenylbicyclo[3.1.0]hexan-2-one (10).** A solution of 4.51 g (18.2 mmol) of 4,4-diphenylcyclohex-2-enone[28] (**1**) in 1200 mL of benzene was degassed with nitrogen for 1 h and photolyzed in a water-cooled photochemical reactor equipped with a 400 W medium-pressure Hg lamp with the $CuSO_4$ filter solution for 3 h. Concentration in vacuo afforded yellowish oil that was chromatographed on silica gel (column 45.0 × 4.0 cm^2, ethyl acetate−hexane 1:5) to give the

(28) Zimmerman, H. E.; Samuelson, G. E. *J. Am. Chem. Soc.* **1969**, *91*, 5307−5318.
(29) Reich, H. J.; Renga, J. M.; Reich, I. L. *J. Am. Chem. Soc.* **1975**, *97*, 5434−5447.
(30) Greenwald, R.; Chaykovsky, M.; Corey, E. J. *J. Org. Chem.* **1963**, *28*, 1128−1129.
(31) Oxidation was performed according to the procedure given in the following: Mancuso, A. J.; Huang, S.-L.; Swern, D. *J. Org. Chem.* **1978**, *43*, 2480−2482.

following fractions: (a) 2.4 g (60%) of *trans*-5,6-diphenylbicyclo[3.1.0]-hexan-2-one (**10**) as colorless solid, R_f 0.46, which was used for the next step without further purification (the analytical sample was recrystallized from hexane−ether mixture to give colorless prisms, mp 72−74 °C (lit.[32] mp 73−74 °C). ^{1}H NMR ($CDCl_3$) δ 7.45−7.20 (m, 10H), 3.12 (d, J = 9.6 Hz, 1H), 2.68 (d, J = 9.6 Hz, 1H), 2.44−2.36 (m, 2H), 2.15−2.01 (m, 1H), 1.21−1.06 (m, 1H)); (b) 0.44 g of starting enone as colorless oil solidifying upon standing, R_f 0.38; and (c) 1.0 g (25%) of *cis*-5,6-diphenylbicyclo[3.1.0]hexan-2-one as colorless solid, R_f 0.31, with all spectral data corresponding to the literature[32] values.

2,*trans*-5,6-Triphenylbicyclo[3.1.0]hexan-2-ol (11). A solution of phenylmagnesium bromide was prepared from 3.38 g (21.5 mmol) of bromobenzene and 0.53 g (22.0 mmol) of Mg in 35.0 mL of ether. A solution of 3.54 g (14.3 mmol) of *trans*-5,6-diphenylbicyclo[3.1.0]-hexan-2-one (**10**) in 50.0 mL of ether was added dropwise to the solution of the Grignard reagent at room temperature. After the addition was complete, the reaction mixture was stirred for 12 h at room temperature followed by quenching with saturated aqueous NH_4Cl and extracting with ether. The combined organic fractions were washed with water and concentrated NaCl solution and dried over Na_2SO_4. After concentration in vacuo the crude product was purified by column chromatography on silica gel (column 45.0 × 4.0 cm^2, ethyl acetate−hexane 1:4) followed by crystallization from hexane to afford 3.5 g (75%) of colorless crystals, mp 94−96 °C. ^{1}H NMR ($CDCl_3$) δ 7.67−7.59 (m, 2H), 7.51−7.44 (m, 2H), 7.42−7.20 (m, 11H), 2.72 (d, J = 8.7 Hz, 1H), 2.51 (d, J = 8.7 Hz, 1H), 2.50 (dd, J_1 = 13.2 Hz, J_2 = 7.8 Hz, 1H), 2.35−2.18 (m, 1H), 2.15 (s, 1H), 1.83 (dd, J_1 = 13.2 Hz, J_2 = 7.8 Hz, 1H), 1.18−1.05 (m, 1H). HRMS *m*/*e* for [M − H_2O] 308.1565 (calcd for $C_{24}H_{20}$ 308.1568).

***trans*-2,5,6-Triphenylbicyclo[3.1.0]hex-2-ene (12).** A solution of 2.5 g (7.7 mmol) of 2,*trans*-5,6-triphenylbicyclo[3.1.0]hexan-2-ol (**11**) in a mixture of 10.0 mL of pyridine and 30.0 mL of methylene chloride was cooled in an ice−water bath, and a solution of 1.37 g (0.84 mL, 11.5 mmol) of $SOCl_2$ in 4.0 mL of methylene chloride was added dropwise. The reaction mixture was stirred at 0 °C for 3 h. The mixture was then gradually allowed to rise to room temperature, and stirred for an additional 12 h. Then it was diluted with methylene chloride, washed with a 5% solution of HCl and water, and dried over Na_2SO_4. After concentration in vacuo, the residue was subjected to column chromatography on silica gel (column 45.0 × 4.0 cm^2, ethyl acetate−hexane 1:6), and the fraction with R_f 0.54 was collected, which afforded a white solid. Recrystallization from hexane gave 1.1 g (47%) of colorless cotton-like crystals, mp 103−105 °C. ^{1}H NMR analysis showed the product to be mixed crystals of *trans*-2,5,6-triphenylbicyclo-[3.1.0]hex-2-ene (**12**) and 1,3,4-triphenylcyclohex-1,4-diene (**15**) in approximate ratio 1:1. ^{1}H NMR ($CDCl_3$) δ 7.65−7.59 (m, 2H of **12**), 7.46−7.05 (m, 13H of **12** + 15H of **15**), 6.36 (tm, J = 4.0 Hz, 1H of **15**), 6.28 (dt, J_1 = 4.4 Hz, J_2 = 1.5 Hz, 1H of **15**), 5.65 (t, J = 2.7 Hz, 1H of **12**), 4.74−4.63 (m, 1H of **15**), 3.47−3.38 (m, 2H of **15**), 3.05 (dd, J_1 = 7.8 Hz, J_2 = 2.7 Hz, 1H of **12**), 2.96 (dd, J_1 = 19.0 Hz, J_2 = 2.7 Hz, 1H of **12**), 2.82 (d, J = 7.8 Hz, 1H of **12**), 2.64 (dt, J_1 = 19.0 Hz, J_2 = 2.7 Hz, 1H of **12**). ^{13}C NMR ($CDCl_3$) δ 145.43, 143.83, 141.91, 140.93, 140.54, 137.41, 136.48, 135.62, 131.48, 130.47, 128.52, 128.50. 128.46, 128.31, 128.26, 128.07, 127.85, 127.13 (2C), 127.09, 126.79, 126.76, 126.28, 126.23, 126.19, 125.94 (2C), 125.12, 123.92, 123.52, 45.88, 39.28, 37.97, 37.27, 35.17, 29.54.

1,*endo*-4,*endo*-6-Triphenylbicyclo[3.1.0]hexan-*exo*-3-ol (13). A solution of 0.95 g (3.1 mmol) of mixed crystals obtained in the previous step in 15.0 mL of anhydrous THF was treated with a solution of BH_3−THF complex (10.8 mL of 1.0 M solution in THF, 10.8 mmol) at ice-bath temperature followed by stirring at this temperature for 2.5 h, and for an additional 2.5 h at room temperature. The resulting mixture was cooled to 0 °C and carefully treated with 3.0 mL of a 10% solution of water in THF followed by addition of 20.5 mL of 3.0 M aqueous NaOH (2.46 g, 61.6 mmol) and 16.5 mL (18.2 g, 0.16 mol) of 30% H_2O_2. The resulting mixture was stirred for 1.5 h at room temperature, poured into 10% aqueous HCl, and extracted with a sufficient amount of ether (2 × 250 mL). The organic fraction was washed with water and brine and dried over Na_2SO_4. Solvents were concentrated in vacuo to a volume of approximately 5.0 mL to afford a white precipitate that was filtered. The clear filtrate was concentrated in vacuo to give a yellow oil, which was chromatographed on silica gel (column 50.0 × 2.5 cm^2, ethyl acetate−hexane 1:5). The fraction with R_f 0.28 was collected and afforded 0.38 g (38%) of alcohol **13** as a colorless oil. ^{1}H NMR ($CDCl_3$) δ 7.45−7.00 (m, 13H), 6.91−6.83 (m, 2H), 3.74 (dd, J_1 = 8.4 Hz, J_2 = 4.4 Hz, 1H), 3.49−3.37 (m, 1H), 2.83 (dd, J_1 = 12.8 Hz, J_2 = 6.9 Hz, 1H), 2.57 (dd, J_1 = 8.7 Hz, J_2 = 4.4 Hz, 1H), 2.50 (d, J = 8.7 Hz, 1H), 2.36 (dd, J_1 = 12.8, J_2 = 8.1 Hz, 1H), 1.55 (br. s, 1H). ^{13}C NMR ($CDCl_3$) δ 145.13, 141.12, 136.82, 130.21, 128.48, 128.06, 127.93, 127.34, 126.43, 126.37, 126.18, 125.93, 72.63, 51.66, 41.10, 33.91, 33.88, 32.18. IR (neat) cm^{-1}: 3550−3150. The white precipitate previously filtered was recrystallized from methanol−THF mixture (2:1) to give 0.27 g (25%) of 2,3,5-triphenylcyclohexan-1,4-diol (**35**) as colorless microcrystals, mp 259−261 °C. ^{1}H NMR (CD_3OD) δ 7.50−6.90 (m, 15H), 4.71 (t, J = 11.1 Hz, 1H), 4.03 (narrow m, 1H), 3.71 (dd, J_1 = 10.8 Hz, J_2 = 5.4 Hz, 1H), 3.45−3.20 (partially overlaping with an OH signal from the solvent, m, 2H + possibly 2H from OH), 2.46 (td, J_1 = 14.7 Hz, J_2 = 2.7 Hz, 1H), 1.99 (dm, J = 14.7 Hz, 1H). HRMS *m*/*e* for [M − 2H_2O − H_2] 306.1410 (calcd for $C_{24}H_{18}$ 306.1410).

1,*exo*-4,*endo*-6-Triphenylbicyclo[3.1.0]hexan-3-one (14). To a solution of 0.27 g (0.72 mmol) of Dess−Martin periodinane[33] in 25.0 mL of CH_2Cl_2 was added pyridine (0.047 g, 0.60 mmol), and the resulting mixture was stirred for 10 min at room temperature. A solution of 100 mg (0.31 mmol) of alcohol **23** in 5.0 mL of CH_2Cl_2 was added dropwise, and the resulting mixture was stirred for 6 h at room temperature. Then it was cooled to 0 °C, and a mixture of 20.0 mL of a 5% aqueous solution of $Na_2S_2O_3$ and 12.0 mL of a concentrated aqueous solution of $NaHCO_3$ was added followed by stirring for an additional 45 min. The resulting solution was diluted with ether, the organic layer separated, and the aqueous layer extracted with ether. The combined organic fractions were washed with water and dried over Na_2SO_4. Concentration in vacuo afforded a yellowish oil. This was treated with sodium ethoxide solution (prepared from 0.077 g (3.35 mmol) of Na and 4.0 mL of EtOH) for 8 h at room temperature. The reaction mixture was diluted with ether, washed with water, dried over Na_2SO_4, and concentrated in vacuo to afford a dark oil, which was purified by preparative plate TLC (silica gel, eluent ethyl acetate−hexane 1:5). The R_f 0.39 band gave 0.06 g (60%) of 1,*exo*-4,*endo*-6-triphenylbicyclo[3.1.0]hexan-3-one (**14**) as a colorless oil. All the spectral characteristics were in agreement with those of the photoproduct **14** obtained in a solid-state preparative photolysis of enone **18**.

Exploratory Solid-State Photolysis of Enone 9. Summarized results of some separate runs are presented in Table 9.

Table 9. Amounts of Photoproducts **16** and **17** vs Total Conversion in the Solid-State Reaction of Enone **9**[a]

	conversion								
	0.05	0.06	0.075	0.08	0.10	0.11	0.17	0.29	0.39
product **16**	0.025	0.03	0.038	0.04	0.05	0.07	0.11	0.25	0.37
product **17**	0.025	0.03	0.038	0.04	0.05	0.04	0.06	0.04	0.02

	conversion					
	0.53	0.63	0.70	0.79	0.91	1.00
product **16**	0.50	0.61	0.69	0.79	0.91	1.00
product **17**	0.03	0.02	0.01	0	0	0

[a] All the amounts are in fractions of unity.

(32) Zimmerman, H. E.; Albrecht, F. X.; Haire, M. J. *J. Am. Chem. Soc.* **1975**, *97*, 3726−3740.

(33) Dess, D. B.; Martin, J. C. *J. Org. Chem.* **1983**, *48*, 4155−4156.

Table 10. Amounts of Photoproducts **17** and **18** vs Total Conversion in the Solid-State Reaction of Enone **13**[a]

	conversion												
	0.01	0.03	0.04	0.065	0.07	0.11	0.145	0.21	0.24	0.30	0.31	0.40	0.42
product **14**	0	0	0	0	0	0	0.043	0.09	0.10	0.15	0.16	0.23	0.24
product **21**	0.01	0.03	0.04	0.065	0.07	0.11	0.102	0.12	0.14	0.15	0.15	0.17	0.18

	conversion						
	0.47	0.51	0.57	0.62	0.66	0.66	0.77
product **14**	0.29	0.32	0.38	0.42	0.47	0.46	0.58
product **21**	0.18	0.19	0.19	0.20	0.19	0.20	0.19

[a] All the amounts are in fractions of unity.

Exploratory Solid-State Photolysis of 4,5,5-Triphenylcyclohex-2-enone (18). Summarized results of some separate runs are presented in Table 10.

Preparative Solid-State Photolysis of 4,5,5-Triphenylcyclohex-2-enone (18). A portion of 1.0 g (3.09 mmol) of crystalline enone **18** was irradiated between two quartz plates (diameter 14 cm) for 100 h. A part (0.7 g) of the reaction mixture was separated by column chromatography on silica gel (column 50.0 × 2.5 cm^2, eluent ethyl acetate−hexane 1:8) to give the following fractions: (a) 25 mg of unidentified yellow oil, R_f 0.60; (b) 95 mg (14%) of *exo*-2,*trans*-5,6-triphenylbicyclo[3.1.0]hexan-3-one (**14**) as colorless oil, R_f 0.42. ^{1}H NMR ($CDCl_3$) δ 7.50−6.90 (m, 15H), 3.70 (s, 1H), 3.06 (d, J = 18.7 Hz, 1H), 2.88 (d, J = 8.6 Hz, 1H), 2.80 (d, J = 18.7 Hz, 1H), 2.66 (d, J = 8.6 Hz, 1H). ^{13}C NMR ($CDCl_3$) δ 212.72, 143.29, 138.30, 133.35, 131.07, 128.96, 128.92, 128.84, 127.37, 127.29, 127.22, 126.50, 125.86, 55.59, 41.53, 35.41, 32.52, 31.96. IR (neat) cm^{-1}: 1745.8. HRMS *m*/*e* 324.1525 (calcd for $C_{24}H_{20}O$ 324.1514); (c) 100 mg (14%) of 4,4,*endo*-6-triphenylbicyclo[3.1.0]hexan-2-one (**21**) as a colorless solid, R_f 0.33, whcih was recrystallized from an ethyl acetate−hexane mixture to give colorless prisms, mp 161−162 °C (lit.[34] mp 161−162 °C). ^{1}H NMR ($CDCl_3$) δ 7.40−7.10 (m, 10H), 7.6 (t, J = 6.9 Hz, 1H), 6.95 (t, J = 6.9 Hz, 2H), 6.70 (d, J = 6.9 Hz, 2H), 3.18 (dd, J_1 = 8.6 Hz, J_2 = 5.4 Hz, 1H), 3.02 (t, J = 8.6 Hz, 1H), 2.73 (dd, J_1 = 8.6 Hz, J_2 = 5.4 Hz, 1H), 2.41 (d, J = 17.5 Hz), 2.17 (d, J = 17.5 Hz); and (d) 420 mg (60%) of starting material as a colorless solid, R_f 0.28.

Preparative Solution Photolysis of 3-*tert*-Butyl-5,5-diphenylcyclohex-2-enone (4). A solution of 60 mg (0.20 mmol) of enone **4** in 40.0 mL of benzene was irradiated in a Pyrex tube placed next to a water-cooled medium-pressure mercury lamp equipped with 2 mm Pyrex filter for 12 h. Nitrogen was passed through the solution during the photolysis. After rotary evaporation of the solvent, the oily residue was separated by column chromatography on silica gel (column 35.0 × 1.5 cm^2, eluent ethyl acetate−hexane 1:6) to give the following fractions: (a) 5 mg (8%) of unidentified product as a colorless oil, R_f 0.89; (b) 12 mg (20%) of 3-*tert*-butyl-2,5-diphenylcyclohex-2-enone (**24**) as a colorless oil solidifying upon standing, R_f 0.62, which was recrystallized from hexane to give colorless thin needles, mp 141−143 °C. ^{1}H NMR ($CDCl_3$) δ 7.49−7.19 (m, 9H), 7.01 (s, 1H), 3.88 (tdd, J_1 = 12.2 Hz, J_2 = 5.4 Hz, J_3 = 1.8 Hz, 1H), 3.25 (t, J = 12.2 Hz, 1H), 2.91 (dd, J_1 = 12.2 Hz, J_2 = 5.4 Hz, 1H), 2.49 (d, J = 12.2 Hz, 1H), 2.38 (t, J = 12.2 Hz, 1H), 0.90 (s, 9H); HRMS *m*/*e* 304.1812 (calcd for $C_{22}H_{24}O$ 304.1827); (c) 21 mg (35%) of a mixture of bicyclic ketones **22** and **23** as a colorless oil, solidifying upon standing, R_f 0.49. Fractional crystallization from methanol afforded 10 mg of 1-*tert*-butyl-*endo*-2,5-diphenylbicyclo[3.1.0]hexan-3-one (**22**) which was additionally recrystallized from hexane to give colorless prisms, mp 171−173 °C. A structure of the product **22** was confirmed by a single-crystal X-ray analysis. Evaporation of the mother liquor gave 8 mg of 1-*tert*-butyl-*exo*-2,5-diphenylbicyclo[3.1.0]hexan-3-one (**23**) as a colorless oil. ^{1}H NMR for **22** ($CDCl_3$) δ 7.50−7.44 (m, 2H), 7.39−7.21 (m, 8H), 4.34 (s, 1H), 3.15 (dt, J_1 = 19.2 Hz, J_2 = 1.9 Hz, 1H), 2.73 (d, J = 19.2 Hz, 1H), 1.92 (dt, J_1 = 6.4 Hz, J_2 = 1.9 Hz, 1H), 1.11 (d, J = 6.4 Hz, 1H), 0.67 (s, 9H); HRMS (FAB with Na^+) *m*/*e* 327.1714 (calcd for $C_{22}H_{24}ONa$ 327.1725). ^{1}H NMR for **23** ($CDCl_3$) δ 7.60−7.00 (m, 10H), 3.62 (s, 1H), 3.39 (dm, J = 18.3 Hz, 1H), 2.73 (d, J = 18.3 Hz, 1H), 1.87 (dd, J_1 = 6.3 Hz, J_2 = 3.3 Hz, 1H), 0.62 (s, 9H), 0.41 (d, J = 6.3 Hz, 1H); HRMS (FAB with Na^+) *m*/*e* 327.1718 (calcd for $C_{22}H_{24}ONa$ 327.1725); and (d) 15 mg (25%) of starting enone as a colorless oil, R_f 0.33.

Exploratory Sensitized Photolysis of 3-*tert*-Butyl-5,5-diphenylcyclohex-2-enone (4). A solution of 6 mg (0.02 mmol) of enone **4** and 30 mg (0.25 mmol) of acetophenone in 2.5 mL of C_6D_6 was irradiated in a NMR tube with a Pyrex filter for 5 h. During the photolysis nitrogen was passed through the solution. ^{1}H NMR analysis showed the ratio of two products **22** and **23** to be 1:1 at the conversion 70%.

Preparative Solid-State Photolysis of 3-*tert*-Butyl-5,5-diphenylcyclohex-2-enone (4). Two portions (25 mg each) of crystalline **4** were irradiated for 2 h at 0 °C. The combined portions were subjected to column chromatography on silica gel (column 35.0 × 1.5 cm^2, eluent ethyl acetate−hexane 1:6) to give the following fractions: (a) 28 mg (56%) of 1-*tert*-butyl-*endo*-2,5-diphenylbicyclo[3.1.0]hexan-3-one (**22**), R_f 0.49; and (b) 18 mg (36%) of the starting material, R_f 0.33.

Preparative Solid-State Photolysis of 3-^{13}C-2-Methyl-4,4-diphenylcyclohex-2-enone (*^{13}C*-9). A 50 mg (0.19 mmol) portion of crystalline ^{13}C-labeled enone ***^{13}C*-9** was irradiated for 29 h. The crystals after irradiation were subjected to column chromatography on silica gel (column 35.0 × 0.9 cm^2, eluent ethyl acetate−hexane 1:5) to afford the following fractions: (a) 45 mg of a mixture of starting material and bicyclic product ***^{13}C*-16**; and (b) 3 mg (6%) of 2-methyl-3-diphenyl-^{13}C-methylcyclopent-2-enone (***^{13}C*-17**) as a colorless oil, R_f 0.28, which was crystallized from pentane to afford colorless crystals, mp 64−67 °C. ^{1}H NMR ($CDCl_3$) δ 7.38−7.11 (m, 10H), 5.44 (d, J = 126.3 Hz, 1H), 2.49−2.38 (m, 4H), 1.69 (s, 3H). HRMS *m*/*e* 263.1374 (calcd for $^{13}CC_{18}H_{18}O$ 263.1391).

Fraction 1 was additionally separated by preparative TLC on a plate, eluted with ethyl acetate−hexane 1:5 to afford the following fractions: (a) 5 mg (10%) of 6-^{13}C-1-methyl-*trans*-5,6-diphenylbicyclo-[3.1.0]hexan-2-one (***^{13}C*-16**) as a colorless solid, R_f 0.54, which was recrystallized from methanol to afford colorless crystals, mp 139−141 °C. ^{1}H NMR ($CDCl_3$) δ 7.43−7.21 (m, 10H), 3.00 (d, J = 157.2 Hz, 1H), 2.34−2.22 (m, 2H), 2.06 (dt, J_1 = 19.2 Hz, J_2 = 5.1 Hz, 1H), 1.22 (d, J = 3.6 Hz, 3H), 1.10 (dt, J_1 = 19.2 Hz, J_2 = 8.7 Hz, 1H). HRMS *m*/*e* 263.1380 (calcd for $^{13}CC_{18}H_{18}O$ 263.1391); and (b) 33 mg of starting material as a colorless solid, R_f 0.46.

Conversion Dependence of Solid-State Quantum Yield. A method used by Zimmerman et al.[4b] was used to determine solid-state quantum yield. Ten to twenty milligram portions of fine crystalline powder of enone were used in each run. The photoproducts ratio was analyzed by ^{1}H NMR. The data obtained are summarized in Table 11.

Computational Procedures. Ab initio, DFT, and combined QM/MM computations were performed on an Intel Pentium III based multiprocessor cluster with Linux OS using the Gaussian 98[11] computational package. Molecular mechanics computations were performed with

(34) Zimmerman, H. E.; O'Brien, M. E. *J. Org. Chem.* **1994**, *59*, 1809−1816.

Table 11. Conversion Dependence of Solid-State Quantum Yield for Enone **18**[a]

	conversion				
	1.5%	3.8%	3.9%	5.2%	12.0%
Φ of product **14**	4.73×10^{-4}	5.07×10^{-4}	2.40×10^{-4}	1.43×10^{-4}	1.16×10^{-4}
Φ of product **21**					4.79×10^{-5}
Φ total	4.73×10^{-4}	5.07×10^{-4}	2.40×10^{-4}	1.43×10^{-4}	1.64×10^{-4}

[a] Irradiation at 320 nm.

MacroModel 6.5[35] using the MM3* force field. Minicrystal lattices were generated based on X-ray data for reactant using Smartpack program.[5b]

General Procedure for Computational Treatment of the Mini-Crystal Lattice. A central molecule was chosen, and a first shell of closest surrounding molecules was defined (all the other more remote molecules were considered as a second shell). Conversion of the central molecule to a reacting intermediate was performed by creating new bonds to be formed and deleting bonds to be broken followed by MM optimization in frozen shells. This was followed by MM optimization of the reacting intermediate together with the first shell inside the frozen second shell (a force constant of 30 kJ/Å was chosen for optimization of the first shell). In some cases it was necessary to use additional constraints to prevent unrealistically strong bending of migrating phenyl group in the central reacting molecule. The optimized central molecule and first shell were extracted and further optimized by ONIOM. In this computation the central molecule was subjected to ab initio optimization, and the first shell was treated by MM (using the Dreiding force field) and kept frozen throughout the entire optimization.

Computational Details. Optimization of intermediates **16T$_{cr}$** and **25T$_{cr}$**: shell 1−14 molecules, shell 2−87 molecules.

Optimization of intermediates **16T$_{cr}$′** and **25T$_{cr}$′** was performed together with one molecule of neighboring cyclopentenone product **17** in each case, i.e., a central part included 2 molecules to be optimized (for ONIOM treatment one molecule (**16T$_{cr}$′** or **25T$_{cr}$′**) was optimized by ab initio, and one molecule of **17** by MM), shell 1−20 molecules, and shell 2−80 molecules.

Optimization of intermediates **27T** and **30T**: shell 1−14 molecules, shell 2−60 molecules.

Optimization of intermediates **27T** and **30T** for a second stage of the solid-state reaction was performed together with 2 neighboring molecules of photoproduct **14**, i.e., a central part included 3 molecules to be optimized (in ONIOM treatment one molecule (**27T** or **30T**) was optimized by ab initio, and two molecules of **14** by MM), shell 1−26 molecules (20 molecules for ONIOM optimization), shell 2−84 molecules.

Acknowledgment. Support of this research by the National Science Foundation is gratefully acknowledged with special appreciation for its support of basic research.

Supporting Information Available: X-ray coordinates of compounds **4** and **22** (PDF). This material is available free of charge via the Internet at http://pubs.acs.org.

JA0124562

(35) Mohamadi, F.; Richards, N. G. J.; Guida, W. C.; Liskamp, R.; Lipton, M.; Caufield, C.; Chang, G.; Hendrickson, T.; Still, W. C. *J. Comput. Chem.* **1990**, *11*, 440−467.